Simulating Hypervelocity Impacts to Monolithic High-Density Polyethylene Plates

Paul T. Mead[a], Jacob A. Rogers[a], T. Neil Williams[b], Justin W. Wilkerson[a], Thomas E. Lacy, Jr.[a,*]

[a] *J. Mike Walker '66 Department of Mechanical Engineering, Texas A&M University, College Station, Texas, 77843.*
[b] *Geotechnical and Structures Laboratory, U.S. Army Engineer Research and Development Center, Vicksburg, MS 39180, USA*

Abstract

Thermoplastic polymers as intermediate layers in protective structures could offer hypervelocity impact (HVI) damage resistance without compromising on weight and cost. Moreover, the ability to accurately simulate the ultra-high strain rate response of polymers would enable protective structure development and optimization. In a previous study, HVI experiments were performed using a two-stage light gas gun to probe the HVI response of high-density polyethylene (HDPE). 6.35 mm thick, monolithic, square targets were subjected to a series of normal, 2.0–6.5 km/s, 10 mm diameter aluminum sphere HVIs. The debris cloud tip velocity, perforation radius, and target mass loss were found to increase with impact velocity. High-speed images displayed apparent HVI-induced bulk melting and large-scale plastic deformation in the HDPE targets. In the current study, the HVI experiments were simulated using established material models and equations of state (EOS) in the Elastic Plastic Impact Computation (EPIC) code. Appropriate material model and EPIC code simulation parameters were calibrated to improve the correlation of HVI damage metrics (*e.g.*, damage morphology, debris cloud geometry and velocity). The simulation results agree well with the experiments across most of the tested velocity regime and provide useful data to help infer the extreme target strain rates and temperatures induced by HVIs.

Keywords: hypervelocity impact, high-density polyethylene, ultra-high strain rate, impact simulation

1. Introduction and Motivation

The mechanical behavior of polymers is highly dependent on temperature, strain, and strain rate, as well as manufacturing and processing history. These sensitivities, however, could potentially be leveraged to develop the next generation of protective materials and structures for space applications (*e.g.*, micrometeoroid/orbital debris protection) [1, 2]. Moreover, tuned thermoplastic polymeric materials as intermediate layers in protective structures could offer hypervelocity impact (HVI) damage resistance while also provid-

*Corresponding author. J. Mike Walker '66 Department of Mechanical Engineering, Texas A&M University, College Station, Texas, 77843, United States.
Email address: telacyjr@tamu.edu (Thomas E. Lacy, Jr.)

ing potential weight and cost savings. The ability to accurately simulate the macroscopic ultra-high strain rate response of polymers would accelerate protective structure development and optimization. Accurately modeling the high- and ultra-high-strain rate response of materials, however, is generally challenging due to HVI-induced irreversible phenomena, including projectile and target erosion, penetration and/or perforation, inelasticity, fracture, melting, spallation, fragmentation, *etc.* [3]. Often, the development and validation of material models and the assessment of simulation techniques requires direct comparison to full-scale HVI experimental results. A significant portion of the HVI/penetration mechanics literature consists of empirical, analytical, and numerical studies on metals. Investigations on non-metallatic materials have been generally less frequent, focusing on composites [4–6], ceramics [7], and other materials [8].

Interest in thermoplastics, specifically polyethylene (PE) and PE composites, has recently increased due to their attractive energy absorption features [1, 9–13]. In addition, these polymers can be additively manufactured and potentially tuned for anticipated impact threats. Even so, numerical predictions of the HVI and ultra-high rate response of PE have been relatively unexplored, especially at higher velocities (and strain rates). This gap in understanding is due, in part, to (*i*) metals being the primary materials used in conventional protective structures, (*ii*) the difficulty associated with systematically generating ultra-high strain rates, and (*iii*) the complexity of polymer-microstructure-induced material behavior. The relatively low-rate material behavior of PE has been well characterized; however, findings at lower rates cannot necessarily be extrapolated to higher strain rates consistent with HVIs. Thus, the problem at hand is three fold: (*i*) characterizing the HVI response of polyethylene (PE) *via* experimentation, (*ii*) using empirical data to inform applicable material models and equation of state (EOS) for practical simulation and optimization efforts, and (*iii*) developing a fundamental understanding of how intrinsic polymeric chemistry, microstructure and morphology influence the macroscopic damage formation and evolution.

Despite these challenges, some work has been done to model and simulate the low- and high-velocity (<3.0 km/s) impact response of thermoplastics, specifically PE. For example, Shah *et al.* [14] developed numerical models for high-density PE (HDPE) and low-density PE (LDPE) substrates each impacted by a 50 μm-diameter polymer particle traveling at 0.2 km/s. This study was performed to develop a better understanding of the cold spray deposition of polymer substrates, which is important for coating surfaces. Pundhir *et al.* [15] used ANSYS Autodyn® and a Johnson-Cook (JC) strength model with orthotropic softening failure criteria to simulate the impact response of a 200 x 200 mm, polymer composite plate (5-9 mm-thick) comprised of HDPE and ultra-high molecular weight PE (UHMWPE) subjected to a steel ogive projectile impact at 0.85 km/s. Simulation results showed that a higher percentage of UHMWPE led to larger energy transfer to the target and greater Von Mises stress in the target at the velocities tested. Austin [16] simulated 2.1 and 3.5 km/s impacts to UHMWPE using ANSYS Autodyn® for comparison with gas gun experiments to improve model accuracy through considering thermal softening, not successfully accounted for in previous UHMWPE models. The model led to simulation results that were more consistent with experimental results while minimizing computational time. Ramezami *et al.* [17] focused on developing an UHMWPE hydrocode model to improve ballistic efficiency and minimize the failure of equipment used in armor and security applications. UHMWPE, specifically 5.5–16.2 mm thick, Dyneema® HB26, panels were numerically impacted by 7.62 mm x 39 mm projectiles at approximately 0.68 km/s. The corresponding results suggest that improvements could be made to modeling techniques for impacts with common battlefield projectiles at these velocities. Several other studies have also conducted similar impact simulations on UHMWPE composites, further exploring their ballistic performance and failure mechanisms, see *e.g.*, [18–22].

The HVI ($\geq$3.0 km/s) response of PE has also been somewhat explored. Bowman *et al.* [23] performed molecular dynamics (MD) simulations of 6 nm thick, PE and polystyrene thin films to analyze the ballistic response of nanoscale materials, which has not been widely investigated and is generally difficult to study experimentally. A relatively large-scale (*e.g.*, millions of atoms) 30 nm spherical projectile impact simulation was performed. A transition was found in the failure mode from petalling to fragmentation as the impact velocity increased from 0.75 km/s to 3 km/s. Also, Bohannan and Fahrenthold [24] used membrane particle-elements to model and simulate the response of 1 mm thick, aluminum-Kevlar targets subjected to 1.68–7.18 km/s HVIs by 2.8 mm and 3.2 mm diameter aluminum spheres. A new modeling method that utilizes membrane particle-elements was developed to address previous inaccuracies associated with modeling techniques for flexible fabrics. Lässig *et al.* [25] modeled and simulated 2.0–6.5 km/s, 6 mm diameter aluminum sphere HVIs to 200 x 200 mm, 0/90° cross-ply Dyneema® HB26 laminate using ANSYS Autodyn®. Two stage light gas gun (2SLGG) experiments were also performed at similar impact velocities to compare with computational results, revealing a slight trend towards over-predicting debris cloud velocity for the model with increasing impact velocity. Lastly, van der Werff *et al.* [26] and others [27] present a plasticity-based model to improve modeling capabilities for HB26 UHMWPE, a layup of SK76 Dyneema® fibers. 3.0–6.0 km/s HVIs to 200 mm x 200 mm and 100 mm x 100 mm targets were simulated with two distinct projectiles: a 6 mm diameter aluminum sphere and a 5.5 mm diameter steel sphere, respectively. Simulation results using this nonlinear plasticity and shock compression model aligned well with experimental results. These relevant results from the literature are qualitatively plotted in impact-velocity-impactor-scale space in Fig. 1, emphasizing simulation conditions yet to be explored. Although the HVI response of UHWMPE has been explored to some degree, the macroscopic HVI response of HDPE has not (to the knowledge of the authors) been numerically simulated.

Rogers *et al.* [28] recently showed experimentally that the HVI response of UHMWPE and HDPE

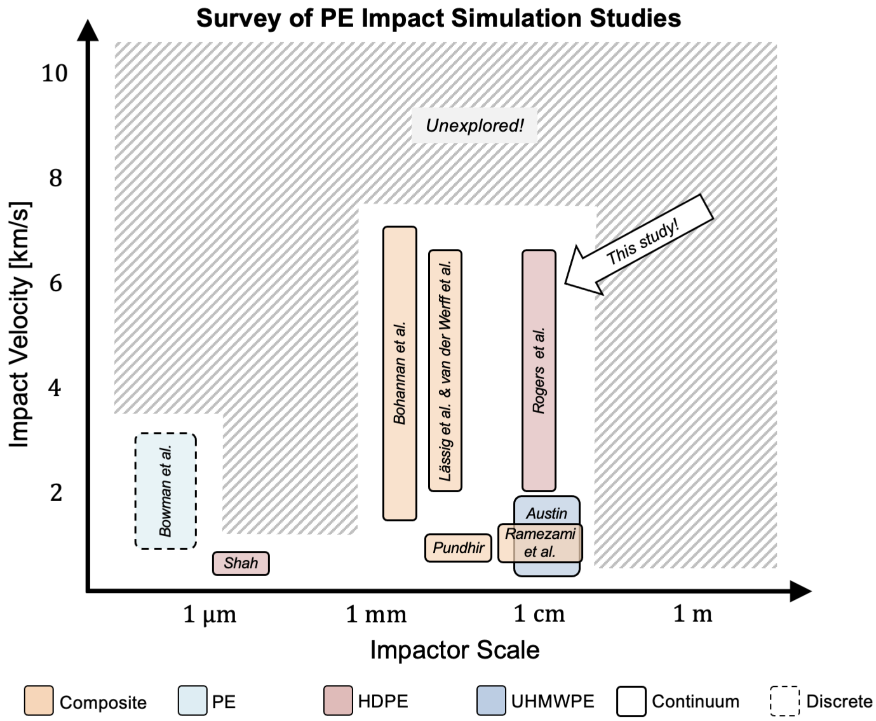

Figure 1: A qualitative representation of relevant literature: numerical simulations of high-rate impacts to polyethylene and polyethylene composites.

differ significantly both macroscopically and microscopically. Monolithic, 6.35 mm thick square plates were subjected to 2.5–6.5 km/s HVIs by a 10 mm diameter 1050 aluminum spheres. UHMWPE was found to fragment in a brittle-like manner (Fig. 2a–c) while HDPE exhibited large-scale melting (Fig. 2d–f). In addition, the HVI-induced perforation radii were larger while the target mass loss was lower in HDPE when compared to similar UHMWPE specimens. For each experiment, the debris cloud *tip* velocity, target mass loss, and perforation radius were found to increase with impact velocity. High-speed images show HVIs to HDPE resulted in apparent bulk-melting of the material and large-scale plastic deformation. Additional material characterization experiments (*e.g.*, DMA, TGA, DSC) were performed to measure key material properties for use in material models. In the current work, the HVI experiments into HDPE presented by Rogers *et al.* [28] were simulated (Fig. 1) using the Elastic Plastic Impact Computation (EPIC) code, a hybrid finite element (FE) and meshless particle computational approach that is well suited for large deformation impact simulations (more later) [29–31]. The preliminary findings of this effort were presented in [32]. Appropriate material model and EPIC code simulation parameters were calibrated to improve the correlation of HVI damage metrics (*e.g.*, damage morphology, debris cloud geometry and velocity). The results show that simulation results agree well with the experiments across a majority of the tested velocity regime. The simulation results were then used to infer local HVI-induced temperatures and strain-rates within the HDPE plates.

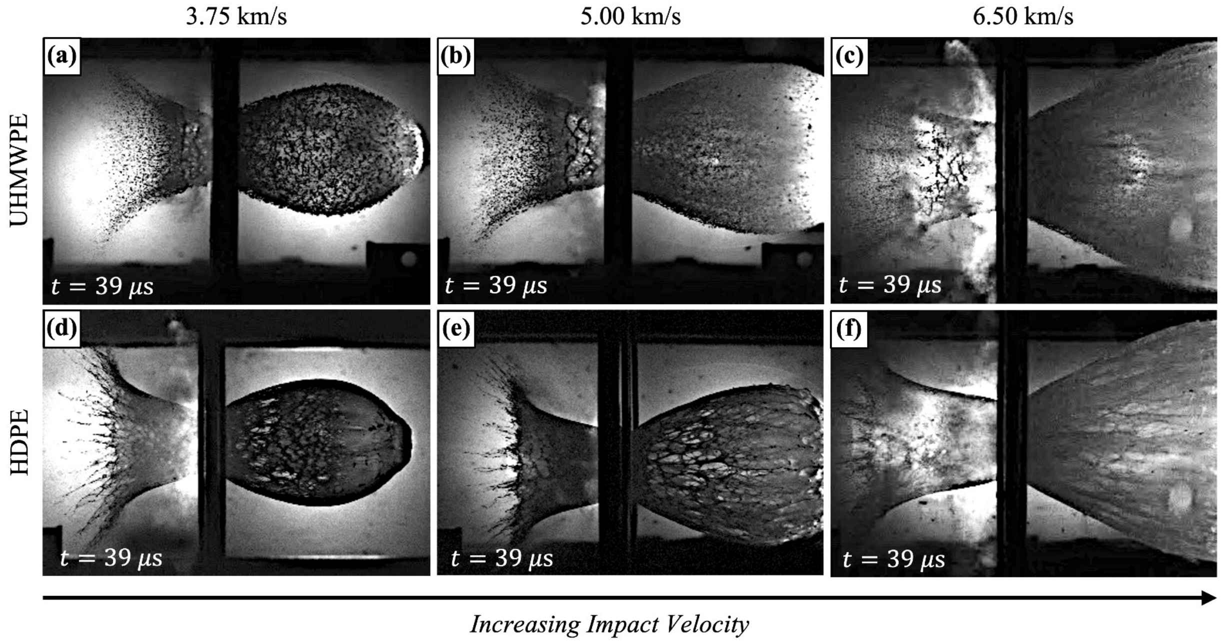

Figure 2: Comparison of fully-developed ejecta and debris clouds at different targeted impact velocities within the tested range: (a-c) for UHMWPE and (d-f) for HDPE. As the targeted impact speed escalates from left to right, the average size of UHMWPE debris fragments reduces, while the extent of melting in HDPE intensifies. Figure reprinted from Ref. [28].

The experimental methodology is briefly presented, followed by a detailed discussion of the simulation approach. Experimental and simulation results are then presented, compared, and discussed. Conclusions are drawn concerning the modeling and simulation approach's validity and limitations in this application, and potential future improvements are suggested.

2. HVI Experimental and Simulation Methodologies

The simulation results presented and discussed in this paper were compared to HVI experimental results. Here, the experimental and simulation methodologies are presented, and the material models and EOS employed are introduced.

2.1. Subjecting HDPE Plates to HVI Using a 2SLGG

The Texas A&M University Hypervelocity Impact Laboratory[1] (HVIL) aeroballistic range 12.7 mm diameter, smooth bore 2SLGG was used to launch the projectiles to the desired hypervelocities [33]. An in-depth discussion of this range and its capabilities is presented in Ref. [33]. The monolithic, HDPE targets were obtained from stock extruded sheets manufactured by King Plastic Corporation ([28, 34]; Table

[1]The HVIL website: `https://telacyjr.engr.tamu.edu/facility/hypervelocity-impact-laboratory-hvil/`.

1). The thickness of all targets was 6.35±0.1 mm, and the in-plane dimensions of the targets were either 15.2 cm x 15.2 cm or 30.5 cm x 30.5 cm. The targets were secured between two apertured, A-36 steel plates using fasteners before being fixed in the target tank. This target fixturing approach effectively induced axisymmetric boundary conditions to facilitate computational simulations. The targets were impacted by 10 mm diameter, 1050 aluminum spheres possessing masses of 1.416±0.004 g. After the HVI experiments, the ultra-high-speed camera images were analyzed using motion tracking software (*e.g.*, Tracker [35]) to determine the debris cloud *tip* velocity. This quantity was calculated across multiple frames and averaged to obtain a nominal value. In addition to these velocity measurements, the ultra-high speed camera images were analyzed qualitatively to determine the bulk material response of the HDPE targets during and after impact. Post-impact analyses included measurements of the perforation radius, target mass loss, and overall damage morphology, as well as scanning electron microscopy (SEM) image evaluation. These results served as quantitative HVI response/damage metrics for the HDPE targets. A more comprehensive presentation and discussion of the experimental methodology and results can be found in Ref. [28].

2.2. Simulating HVIs into HDPE Plates Using EPIC

In this study, a hybrid computational code (EPIC), which uses finite elements and meshless particles to represent large deformations, was used to simulate HVIs into the HDPE targets. Circular targets 6.35 mm-thick and 203 mm in diameter were rendered and meshed in three-dimensional (3D) quarter-symmetry using hexahedral elements. Each hexahedral element was then converted into twenty-four linear tetrahedral elements (Fig. 3). The size and shape of the simulated target was consistent with the axisymmetric region imposed on the experimental targets by the apertured target frame (*cf.* Section 2.1). The target mesh was biased such that the elements increased in size as a function of distance from the point of impact. This biasing was done to increase simulation fidelity while keeping the problem size manageable. Moreover, the 1050 aluminum projectile elements were similar in edge length to those in the contact region (∼0.77 mm). Element-to-particle conversion, a key feature of the EPIC code, was utilized, and the equivalent strain required to convert an element to a particle in both materials was set to 30%, a common conversion strain value for ductile materials [36].

Table 1: Quasi-static material characterization data for HDPE resulting from TGA, DSC, and DMA. The extruded sheets of HDPE were manufactured by King Plastic Corporation. Data reprinted from Ref. [28].

Quantity	Value
Glass transition temperature, T_g (°C)	-116.2 ± 0.8
Melting temperature, T_m (°C)	131.14 ± 0.58
Crystallinity, (%)	70.24 ± 1.98
Density, (g/cc)	0.954 ± 0.002
Initial decomposition temperature, IDT (°C)	423.2

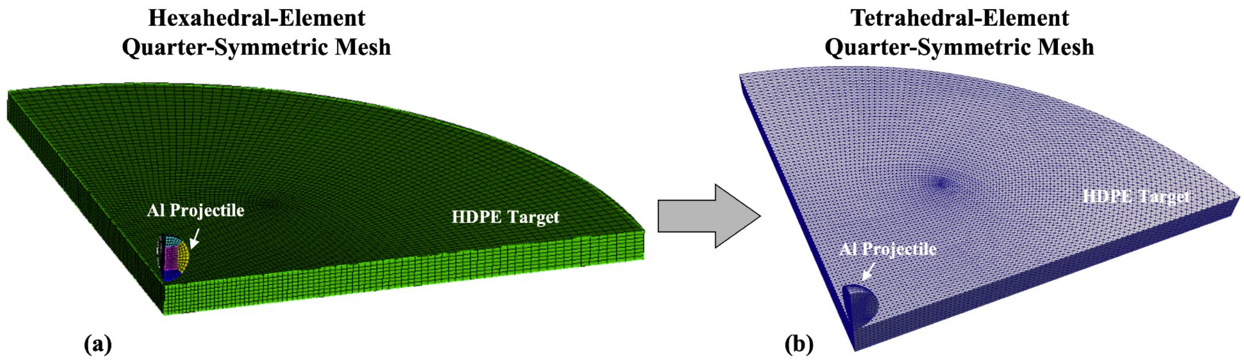

Figure 3: Simulation snapshots showing projectile and target quarter-symmetric meshes before and after the conversion of each hexahedral element into twenty-four tetrahedral elements.

A simple mesh refinement study was performed in 3D quarter symmetry. Specifically, the same impact simulation, a 4 km/s impact, was performed with three different target and projectile mesh refinement levels (roughly 18,000, 119,000, and 950,000 elements total) to observe any potential mesh-induced changes in impact damage metrics (*e.g.*, perforation radius, debris cloud tip velocity, damage morphology). This mesh refinement study showed that the most refined mesh (950,000 elements) and the second most refined mesh (119,000 elements) returned perforation radii that differed by 0.5% (see Fig. A.1), and the corresponding debris cloud tip velocities exhibited similar agreement. Even with this agreement, the more refined mesh was selected for this study in the absence of significant additional computational burden. Specifically, the highest impact velocity simulation (6.5 km/s), which corresponds to the shortest time step, ran to 80 μs in 40 min using the fine mesh geometry on 108 SGI Ice-X 2.6GHz cores. Simulation results using the chosen quarter-symmetric mesh were also compared to similar simulation results using a 3D *half-symmetric* mesh of the same fidelity; no significant differences in debris cloud tip velocity or perforation radius were observed. Hence, the 3D quarter-symmetric mesh of 950,000 elements was chosen for all simulations presented and discussed herein.

Both the aluminum projectile and the HDPE target were modeled using a JC constitutive model [37], a JC fracture model [38], and a Mie-Gruneisen EOS [39]. The HDPE model uses the cubic form of the Mie-Gruneisen EOS; this form can be shown as

$$P = (K_1\mu + K_2\mu^2 + K_3\mu^3)(1 - \Gamma\mu/2) + \Gamma E_s(1 + \mu), \tag{2.1}$$

where P is the pressure, K_1, K_2, and K_3 are polynomial coefficients, Γ is the Gruneisen coefficient, E_s is the internal energy per unit volume, and μ is given by the relationship $\mu = \rho/\rho_0$ - 1 where ρ is the current density and ρ_0 is the initial density. While the Mie-Gruneisen EOS is typically applied to metals, the polyethylene fit from Ref. [40] (see Table 2) is comparable to experimental Hugoniot data for Marlex (a proprietary commercial HDPE), as reported in [41] (see Fig. A.3).

The JC constitutive model gives the material dynamic flow stress (σ) as

$$\sigma = \left(C_1 + C_2\bar{\varepsilon}^N\right)\left(1 + C_3 \ln \dot{\bar{\varepsilon}}^*\right)\left[1 - (T^*)^m\right], \tag{2.2}$$

where C_1 is the yield stress, C_2 is the hardening coefficient, $\bar{\varepsilon}$ is the equivalent plastic strain, N is the hardening exponent, C_3 is the strain rate coefficient, $\dot{\bar{\varepsilon}}^*$ is the dimensionless total equivalent strain rate (normalized by a strain rate of 1 s^{-1}), $T^* = (T - T_0)/(T_m - T_0)$ is the homologous temperature, T and T_0 are the current and reference temperatures, T_m is the melting temperature, and m is the softening exponent. Here, the target temperature is updated at the (i^{th}+1) timestep *via* $T_{i+1} - T_i = \beta\sigma\bar{\varepsilon}/(\rho_0 c_v)$, where $T_{i=1} = T_0$, $\beta = 1$ is the Taylor-Quinney coefficient for HDPE (*i.e.*, fraction of plastic work converted to heat), and c_v is the specific heat capacity of HDPE at a constant volume. The parameters in Eq. (2.2) were adjusted to reflect the actual target and projectile materials used in experimentation. In the case of the 1050 aluminum projectile, the density, yield stress, melting temperature, and shear modulus were adjusted to reflect the values reported by the projectile supplier [42]. For the HDPE target, the density and melting temperature values were adjusted in the model to reflect material characterization results of coupons taken from the HVI-tested specimens [28]. Additionally, to better capture the constitutive response of HDPE, data from a variety of strain rates and temperatures were sourced from Brown *et al.* [43] and were used to calibrate the JC constitutive model constants (see Fig. A.2). In this previous study, quasi-static compression and split Hopkinson pressure bar tests were performed for HDPE specimens across a range of temperatures to record the true stress-true strain relationship for a significant span of strain rates (10^{-4}–10^{3} s^{-1}). The JC constitutive model parameters were chosen to fit the almost perfectly plastic material response observed. These values, as well as other important material parameters are reported in Table 2.

Additionally, a short parametric study was performed to understand the sensitivity effects of JC fracture model coefficients on target perforation radius. A common form of the JC fracture model gives the equivalent strain to fracture (ε_p^f) under constant conditions of $\dot{\bar{\varepsilon}}^*$ (*cf.* Eq. 2.2) as

$$\varepsilon_p^f = \left(D_1 + D_2 e^{D_3\sigma^*}\right)\left(1 + D_4 \ln \dot{\bar{\varepsilon}}^*\right)\left(1 + D_5 T^*\right), \tag{2.3}$$

where D_1–D_5 are fitting parameters, $\sigma^* = \sigma_m/\sigma_{eq}$ is the pressure stress ratio (stress triaxiality [38]), σ_m is the mean normal stress, and σ_{eq} is the equivalent stress. Damage in this equation is defined through the sum of the accumulated equivalent strain divided by ε_p^f. An element or converted particle is considered to be fully damaged or fractured when $\Sigma\Delta\varepsilon_p/\varepsilon_p^f$ reaches a value of unity.

Initially, the spall strength of the HDPE model was adjusted to match data from the literature. Spall can occur within the JC model when average tensile stress (negative pressure) reaches a critical value. The equivalent strain to fracture (ε_p^f) varies linearly from $\sigma^* = 1.5$ to σ^*_{spall} at the minimum strain to failure limit (D_1) where σ^*_{spall}=$\sigma_{spall}/\sigma_{eq}$. The spall strength ($\sigma_{spall}$) for the HDPE model was chosen from the data reported by Jordan *et al.* [44]. The data showed that for three flyer plate impact experiments with velocities ranging from 0.43–0.80 km/s the spall strengths ranged from 50–70 MPa, implying that HDPE spall strength is relatively strain rate independent compared to other polymers. To determine the appropriate spall strength, three HVI simulations at an impact velocity of 6.5 km/s were conducted, adjusting the spall strength of the HDPE target to values report in Ref. [44] (50, 60, and 70 MPa). The impact velocity of 6.5 km/s was selected for the parametric study due to the significant changes in hole size and damage morphology at higher velocities. The simulation results indicated that the spall strength was inversely proportional to the perforation radius, however, the influence was small (<3.3% difference between the 50 and 70 MPa simulations). The simulation with a spall strength of 50 MPa exhibited more petalling on the rear surface of the target compared to experimental observations in Ref. [28], while the simulation with a spall strength of 70 MPa underpredicted the extent of petalling. Based on these results, a spall strength of 60 MPa was selected as it provided the most accurate representation of the observed damage morphology. Additionally, the minimum strain to failure limit, controlled by D_1 [Eq. (2.3)], was reduced from a value of 30% to a value of 5%. This reduction had very little effect on the perforation radius. The negligible repercussions of this

Table 2: Mie-Gruneisen EOS and Johnson-Cook constitutive and fracture model parameters for the for HDPE target.

Parameter	**Value**	**Unit**
Yield stress, C_1	31.27	[MPa]
Hardening coefficient, C_2	0.0	[MPa]
Strain rate coefficient, C_3	0.04	-
Hardening exponent, N	0.75	-
Softening exponent, m	0.85	-
Shear modulus, G	275.8	[MPa]
Specific heat capacity, c_v	2.323	[J/g-°C]
Strain to failure coefficient, D_1	0.05	-
Exponential coefficient, D_2	1.48	-
Stress triaxiality coefficient, D_3	-1.5	-
Strain rate coefficient, D_4	0.25	-
Temperature coefficient, D_5	0.0	-
Spall strength, σ_{spall}	60	[MPa]
Bulk modulus, K_1	7.9	[GPa]
Quadratic M-G Coefficient, K_2	2.296	[GPa]
Cubic M-G Coefficient, K_3	43.36	[GPa]
Gruneisen Coefficient, Γ	0.86	-

change can be attributed to the relatively minimal share of spall-independent material plasticity that comes from high triaxiality during HVI impacts. The effects of changes in strain rate coefficient, D_4, were also investigated: a total of eight HVI simulations were performed where v_0 was changed from 2.0 to 6.5 km/s for each of the four D_4 values investigated. The parametric study showed slight changes in the perforation radii for both the 2.0 and the 6.5 km/s impacts (<2.9% and <1.7%, respectively). The most drastic variation is likely attributed to the detachment of single particles (averaging 0.35 mm in diameter) around the damaged rim of the perforation, increasing the radius slightly. Thus, the value of D_4 was chosen to be 0.25 for the remainder of this study to optimally account for changes in impact-velocity-dependent damage response.

The predicted debris cloud tip velocities, perforation radii, and target mass loss values were calculated using ParaView version 5.5.1 for comparison with experimental results [45]. The debris cloud tip velocity was estimated by averaging the downrange velocities of the converted particle composing the debris cloud tip at a given instant in time. This measurement technique differs slightly from the *experimental* method: experimental debris cloud tip velocities were computed by averaging the downrange tip velocity over time. This approach was necessary to account for minimal debris cloud deceleration induced by atmospheric drag [*i.e.*, some sub-atmospheric pressure (∼100 Torr) existed in the test/target chamber]. The lack of atmospheric drag in the simulations made the time-averaged velocity calculation step unnecessary. In fact, a given converted particle's downrange velocity remained constant unless acted upon by another particle. Thus, the debris cloud tip velocity *simulation* estimation needed to only be performed after sufficient debris cloud expansion to reduce potential particle-particle interactions (a time of 80 μs was found to be sufficient for all impact velocities). The perforation radii were also determined *via* ParaView after the predicted strain rate in the target elements reached a functionally low value (*e.g.*, $\leq 10^{-4}$ s^{-1}) for the highest impact velocity. At this time (roughly 80 μs), a software threshold was placed on the target to hide all particles with an accumulated damage/burn parameter of unity. With this filter in place, the impact perforation radius was measured from the edges of the remaining converted particles that have not been detached from the simulated target. The simulated target mass loss was evaluated in a similar, damage-based manner that would appropriately reflect the experimental measurement methodology to achieve the most consistent results.

3. A Comparison of EPIC Predictions to Experimental Measurements

For this study, impact simulations were executed at six different velocities across the experimentally tested impact velocity regime, $v_0 = 2.0$, 3.0, 4.0, 5.0, 5.5, and 6.5 km/s. The simulation results were postprocessed to determine the debris cloud tip velocity, perforation radius, and target mass loss. Comparing these three

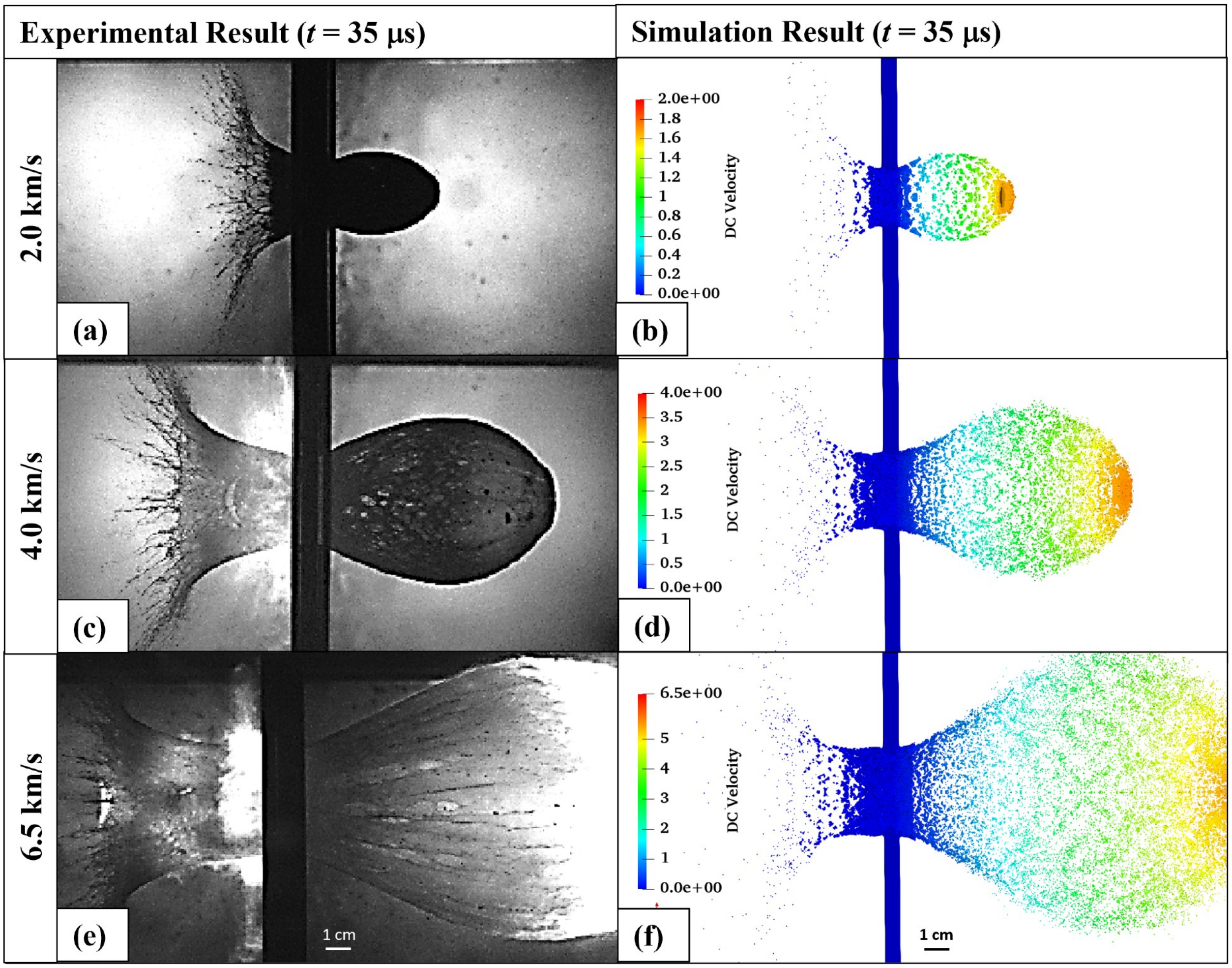

Figure 4: A comparison between experimental high-speed images and simulation snapshots for a 2.0 km/s, a 4.0 km/s, and a 6.5 km/s, 10 mm sphere HVI into 6.35 mm thick HDPE showing differences in debris cloud size and shape development at $t =$ 35 μs: (a)–(b) 2.0 km/s results, (c)–(d) 4.0 km/s results, and (e)–(f) 6.5 km/s results.

parameters to experimental values serves as one simple method to assess the validity of the simulation. Representative experimental high-speed images (Figs. 4a, 4c, and 4e) and time-corresponding simulation snapshots (Figs. 4b, 4d, and 4f) show 10 mm diameter sphere HVIs into a 6.35 mm thick HDPE plates at velocities of 2.0 km/s (Figs. 4a and 4b), a 4.0 km/s (Figs. 4c and 4d), and 6.5 km/s (Figs. 4e and 4f). Each experimental and simulated snapshot was taken 35 μs after impact for this side-by-side comparison. The simulation appears to capture the essential character (size, shape, *etc.*) of the debris cloud across the range of velocities. Some notable differences, however, do exist. For example, the experimental *ejecta* cloud is larger than the predicted cloud, particularly for the 6.5 km/s impact (Fig. 4e and 4f). The simulation also could not precisely capture the fibrous (spider-web-like) features of the melted ejecta and debris clouds reported by Rogers *et al.* [28]. This discrepancy is expected as melting and recrystallization phase transitions, as well as solid-liquid interactions, are difficult to reproduce using FE-SPH computational methods.

Despite these differences, key quantitative metrics between the simulations and experiments agreed quite well for a majority of the investigated velocity regime. The simulated debris cloud tip velocity (Fig. 5a) matched the experimental measurements reasonably well across the entire velocity regime. Except at high velocities ($\geq$ 5.5 km/s), the predicted values tended to be slightly lower than the measured velocities. The simulated perforation radii at impact velocities of 2.0 km/s, 3.0 km/s, 4.0 km/s, and 5.0 km/s are consistent with experimental measurements (Fig. 5b). A noticeable discrepancy, however, exists between the simulated and experimental values at impact velocities >5.0 km/s. The predicted target mass loss (Fig. 5c) agreed reasonably with the experimental data with a slight tendency to over predict target mass loss in the velocity range of 4.0 to 5.0 km/s. These observed discrepancies are likely due to the JC plasticity and fracture models being calibrated using experimental data at strain rates $< 10^4$ s^{-1} (*i.e.*, whereas the average strain rates induced during HVIs likely are on the order of $v_0/h_t \sim 10^5$–10^6 s^{-1}, where h_t denotes target thickness).

Constitutive model insensitivity at ultra-high strain rates is well documented in the literature for a variety of materials (*e.g.*, [3, 46]). In essence, the HVI response of projectile and target materials depends more strongly on density, bulk modulus, projectile/target geometries, and pressure (*i.e.*, EOS) as v_0 (strain rate) increases. Furthermore, a reduction in target performance at roughly 5.5–6.5 km/s (Fig. 5d) has been reported to correspond to a transition from partial to full melt of projectile and target materials for aluminum-on-aluminum impacts [28, 47, 48]. A similar transition could account for the observed decrease in target performance for aluminum-on-HDPE impacts. As impact velocity increases, the heating from adiabatic shock and rapid plastic deformation also rises, potentially causing complete melting of the target material along the projectile path. The simulation results appear to deviate from experimental values as the impact velocity exceeds this transition velocity. The ability to accurately predict target mass loss and debris cloud tip velocity has implications on the prediction capabilities of overall debris cloud momentum and kinetic energy, two key metrics in understanding the protective capabilities of a HVI protective structure. Overall, these simulations are very effective in predicting the perforation radius, target mass loss, debris cloud shape, and debris cloud tip velocity resulting from HVIs to HDPE plates over the impact velocity range $v_0 \approx 2.0$–5.5 km/s at this target-thickness-to-projectile-diameter ratio ($h_t/D \approx 0.635$).

The relatively good agreement motivated the use of simulation results to probe the spatial distributions of HVI-induced target strain rates and temperatures, which cannot yet be readily measured experimentally. Simulation snapshots showing strain rate and temperature distributions at 1.6 μs after 2.0, 4.0, and 6.5 km/s impacts are presented in Figs. 6a–6c and 6d–6f, respectively. Figures 6a, 6b, and 6c provide insight into the strain rates achieved during an HVI event by displaying the strain rates in the simulations as they vary from quasi-static ($<10^{-4}$) to ultra-high strain rate ($>10^6$). A strain rate index showing characteristic regimes is also provided for reference. These strain rates are consistent with observed and/or predicted rates in the

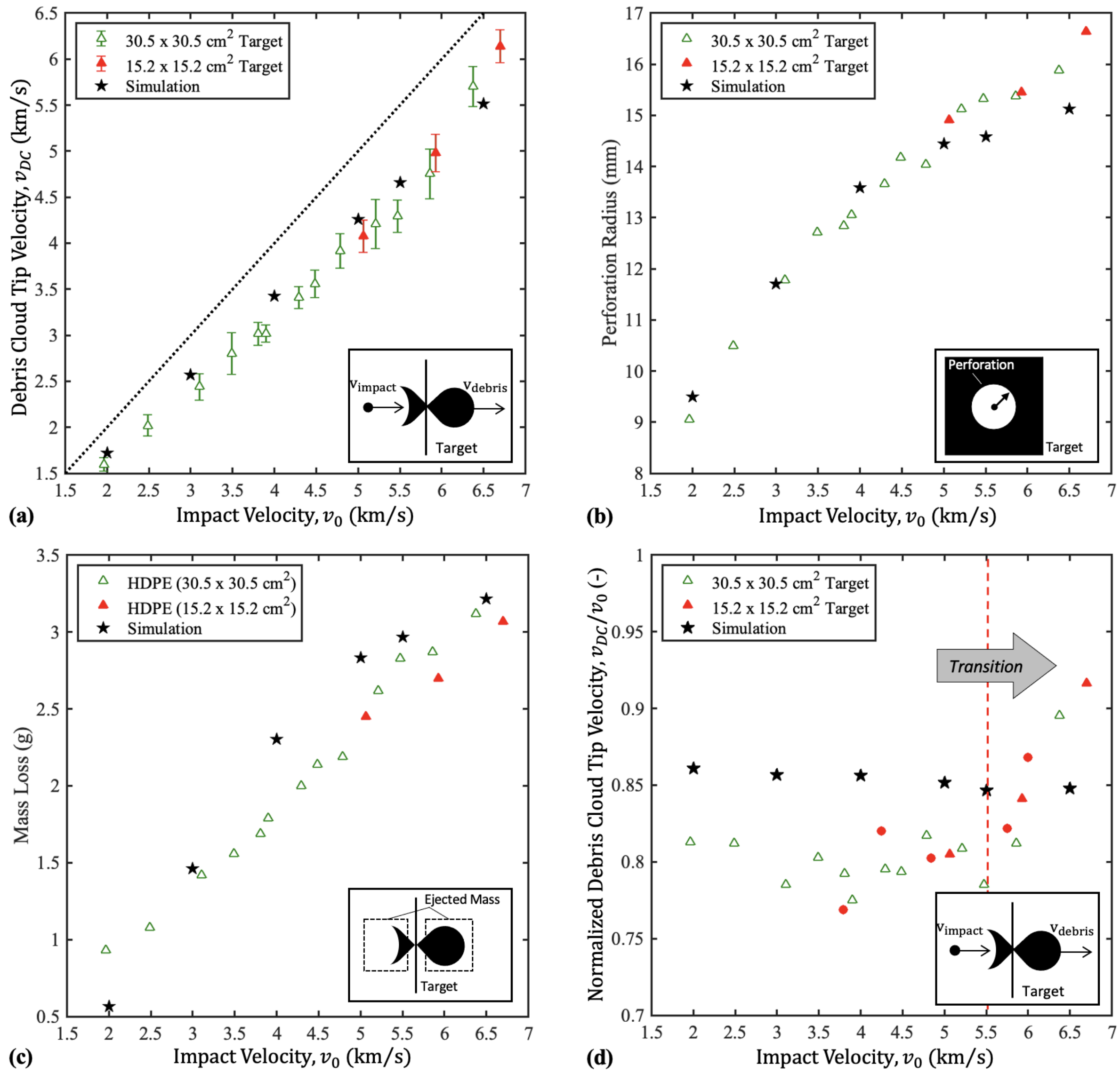

Figure 5: A comparison of simulation and experimental results: the (a) debris cloud tip velocity (v_{DC}), (b) perforation radius, (c) target mass loss, and (d) impact-velocity-normalized debris cloud tip velocity (v_{DC}/v_0) measurements plotted as a function of impact velocity (v_0) for both experiment and simulation. The discrepancies between experiment and simulation roughly correspond to a transition evident in (d), also observed in Ref [28].

literature [49]. Furthermore, these results confirm that the strain rates generated in the simulation exceed the strain rates used to calibrate the JC model's strain rate dependency. There is a tendency for higher strain rates to occur closer to the exit face for this particular target and projectile geometry. To provide even more insight into the extreme conditions developed during HVIs, the temperatures recorded by the simulation are displayed with a scale that ranges from room temperature (22.1°C) to the melting temperature of HDPE (T_m = 131.1°C). The simulation predicts local temperatures sufficient to melt the polymer a very short time after impact (1.6 μs). Extensive melting has also been observed in experimental high-speed camera

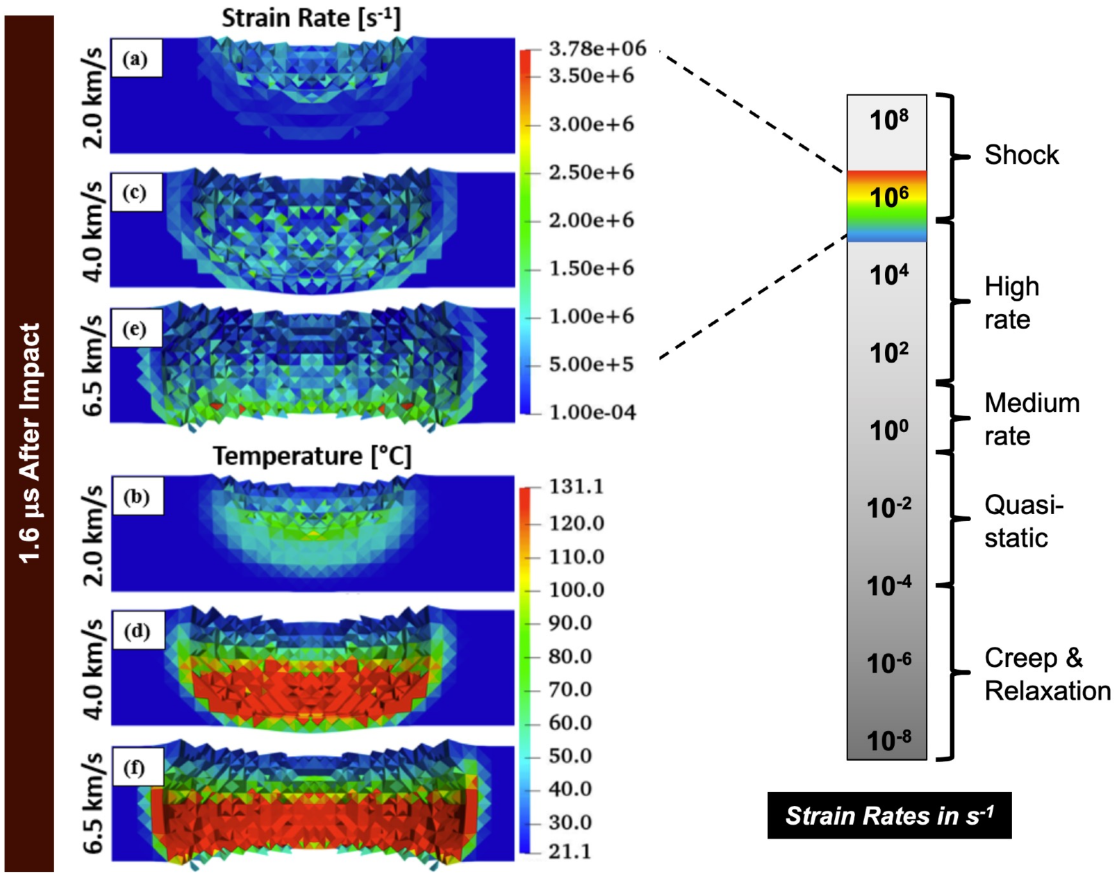

Figure 6: Elemental strain rate and temperature distributions of HDPE targets $t = 1.6$ μs after impact for (a,b) 2.0 km/s, (c,d) 4.0 km/s, and (e,f) 6.5 km/s.

footage of HDPE impacts (Fig. 2d–f) [28]. Note that at $t = 1.6$ μs, the majority of the elements at or above melting temperature exist in the downrange half of the target's thickness. This temperature and strain rate distribution could partially explain why there is a slight increase in perforation radius between the target's impact face and exit face. The ability to accurately predicting through-thickness strain rates and temperatures for a given impact scenario may enable the development of novel polymer protective structures, where the material properties are optimally tuned for the local anticipated HVI-induced strain rates and/or temperatures.

4. Conclusions

The hybrid FE-meshless particle code, EPIC, was used to simulate 10 mm diameter spherical 1050 aluminum projectile HVIs (2.0–6.5 km/s) into 6.35 mm thick HDPE plates. The simulations employed a JC constitutive and fracture model and a Mie-Grüneisen EOS. The constitutive and fracture models were calibrated using material data and relevant data from the literature. Three HVI damage metrics were used to compare experimental and simulation results: debris cloud tip velocity, target perforation radius, and target mass loss. The simulations captured the variation of these three quantities quite well over a large range of the considered impact velocities (2.0–5.0 km/s). Simulation results deviated slightly from experimental data above 5.5 km/s, likely due to inadequate materials data at the corresponding high strain rates (10^6 s^{-1}) and the inability of the Mie-Grüneisen EOS to appropriately predict phase change as impact velocities increased. A transition velocity has been previously reported in other HVI studies. The simulation results were used to infer the HVI-induced spatial distribution of HDPE target strain rates and temperatures over a range of velocities; to the authors' knowledge such predictions have not been previously reported for polyethylene. This crucial spatial data can inform ongoing and future experimental, analytical, and numerical studies.

The ability to reasonably estimate target mass loss and debris cloud geometry and tip velocity simultaneously is particularly useful. In designing novel protective structures, quantifying momentum/energy transfer to underlying structures or assets for a given impact scenario is of paramount importance. Accurate estimates of the momentum and kinetic energy of the ejecta/debris clouds, as well as further investigation into impact geometry effects, could permit the application of this approach to the development of HDPE strain-rate tuned and/or architected spacecraft protection systems. The current study serves as an important step towards that goal.

Declaration of Competing Interest

The authors declare that they have no known competing financial interests or personal relationships that could have appeared to influence the work reported in this paper.

Acknowledgments

This research is based upon work partially supported by the DoD Science, Mathematics, and Research for Transformation (SMART) program. The authors also acknowledge support through the US Army Engineer Research and Development Center (ERDC). The views and conclusions contained in this document are those of the authors and should not be interpreted as representing the official policies, either expressed or implied, of the Army Research Office or the U.S. Government. The U.S. Government is authorized to reproduce and distribute reprints for Government purposes notwithstanding any copyright notation herein.

References

[1] W. P. Schonberg, Studies of hypervelocity impact phenomena as applied to the protection of spacecraft operating in the MMOD environment, Procedia Engineering 204 (2017) 4–42. doi:10.1016/j.proeng.2017.09.723.

[2] E. Christiansen, Micrometeoroid and orbital debris (MMOD) risk overview, Tech. rep., National Aeronautics and Space Administration (NASA), Johnson Space Center (2014).
URL https://ntrs.nasa.gov/archive/nasa/casi.ntrs.nasa.gov/20140009950.pdf

[3] W. Herrmann, J. S. Wilbeck, Review of hypervelocity penetration theories, International Journal of Impact Engineering 5 (1-4) (1987) 307–322.

[4] W. Schonberg, F. Schäfer, R. Putzar, Hypervelocity impact response of honeycomb sandwich panels, Acta Astronautica 66 (3-4) (2010) 455–466.

[5] W. Schonberg, Hypervelocity impact testing of non-metallic materials. 17th cong. intern. council of the aeronaut. sci., sept. 9–14, 1990, at stockholm, sweden, Tech. rep., paper ICAS-90-1.7. 3 (1990).

[6] S. Ryan, F. Schäfer, M. Guyot, S. Hiermaier, M. Lambert, Characterizing the transient response of cfrp/al hc spacecraft structures induced by space debris impact at hypervelocity, International Journal of Impact Engineering 35 (12) (2008) 1756–1763.

[7] N. Kawai, K. Tsurui, D. Shindo, Y. Motoyashiki, E. Sato, Fracture behavior of silicon nitride ceramics subjected to hypervelocity impact, International Journal of Impact Engineering 38 (7) (2011) 542–545. doi:https://doi.org/10.1016/j.ijimpeng.2011.01.003.
URL https://www.sciencedirect.com/science/article/pii/S0734743X11000042

[8] Y. Kim, Y. Park, J. Cha, V. A. Ankem, C.-G. Kim, Behavior of shear thickening fluid (STF) impregnated fabric composite rear wall under hypervelocity impact, Composite Structures 204 (2018) 52–62.

[9] N. Kawai, Y. Kuroda, M. Nagano, S. Hasegawa, E. Sato, Stress-wave propagation and damage formation associated with hypervelocity penetration into polycarbonate, Procedia Engineering 204 (2017) 255–261. doi:10.1016/j.proeng.2017.09.733.

[10] S. Khatiwada, C. A. Armada, E. V. Barrera, Hypervelocity impact experiments on epoxy/ultra-high molecular weight polyethylene fiber composites reinforced with single-walled carbon nanotubes, in: Procedia Engineering, Vol. 58, Elsevier Ltd, 2013, pp. 4–10. doi:10.1016/j.proeng.2013.05.003.

[11] L. H. Nguyen, S. Ryan, S. J. Cimpoeru, A. P. Mouritz, A. C. Orifici, The effect of target thickness on the ballistic performance of ultra high molecular weight polyethylene composite, International Journal of Impact Engineering 75 (2015) 174–183. doi:10.1016/j.ijimpeng.2014.07.008.

[12] A. Bohannan, E. Fahrenthold, Hypervelocity impact simulation using membrane particle-elements, International Journal of Impact Engineering 35 (12) (2008) 1497–1502. doi:10.1016/j.ijimpeng.2008.07.030.

[13] R. Verker, N. Eliaz, I. Gouzman, S. Eliezer, M. Fraenkel, S. Maman, F. Beckmann, K. Pranzas, E. Grossman, The effect of simulated hypervelocity space debris on polymers, Acta Materialia 52 (19) (2004) 5539–5549. doi:10.1016/j.actamat.2004.08.013.

[14] S. Shah, J. Lee, J. P. Rothstein, Numerical simulations of the high-velocity impact of a single polymer particle during cold-spray deposition, Journal of Thermal Spray Technology 26 (5) (2017) 970–984.

[15] N. Pundhir, G. Arora, H. Pathak, S. Zafar, Ballistic impact response of HDPE/UHMWPE polymer composite, in: Advances in Mechanical Engineering, Springer, 2020, pp. 245–255.

[16] S. Austin, A. Brown, J. Escobedo, H. Wang, H. Kleine, P. Hazell, The high-velocity impact of dyneema® and spectra® laminates: implementation of a simple thermal softening model, Procedia Engineering 204 (2017) 51–58.

[17] A. Ramezani, H. Rothe, A new approach to modelling fiber-reinforced plastics for hydrocode analysis, in: SIMUL 2017: The Ninth International Conference on Advances in System Simulation, 2017, pp. 41–50.

[18] B. Ansari, M. K. Hazzard, L. F. Kawashita, U. Heisserer, S. R. Hallett, Numerical modelling of uhmwpe composites under impact loading, in: Twenty second international conference on composite materials (ICCM22), International Committee on Composite Materials, 2020.

[19] T. G. Zhang, S. S. Satapathy, L. R. Vargas-Gonzalez, S. M. Walsh, Ballistic impact response of ultra-high-molecular-weight polyethylene (uhmwpe), Composite structures 133 (2015) 191–201.

[20] M. K. Hazzard, R. S. Trask, U. Heisserer, M. Van Der Kamp, S. R. Hallett, Finite element modelling of dyneema® composites: From quasi-static rates to ballistic impact, Composites Part A: Applied Science and Manufacturing 115 (2018) 31–45.

[21] L. H. Nguyen, T. R. Lässig, S. Ryan, W. Riedel, A. P. Mouritz, A. C. Orifici, A methodology for hydrocode analysis of ultra-high molecular weight polyethylene composite under ballistic impact, Composites Part A: Applied Science and Manufacturing 84 (2016) 224–235.

[22] A. J. Carpenter, S. Chocron, C. E. Anderson Jr, Bridging the scales: Continuum-based material constitutive modeling of mechanical and ballistic test data from composites and fabrics, International Journal of Impact Engineering 120 (2018) 31–45.

[23] A. L. Bowman, E. P. Chan, W. B. Lawrimore, J. K. Newman, Supersonic impact response of polymer thin films via large-scale atomistic simulations, Nano Letters 21 (14) (2021) 5991–5997.

[24] A. Bohannan, E. Fahrenthold, Hypervelocity impact simulation using membrane particle-elements, International Journal of Impact Engineering 35 (12) (2008) 1497–1502.

[25] T. Lässig, L. Nguyen, M. May, W. Riedel, U. Heisserer, H. van der Werff, S. Hiermaier, A non-linear orthotropic hydrocode model for ultra-high molecular weight polyethylene in impact simulations, International Journal of Impact Engineering 75 (2015) 110–122.

[26] H. Van der Werff, U. Heisserer, T. Lässig, W. Riedel, New protection levels of UHMWPE armour: From a hydrocode model of HB26 to new generation dyneema® for armour applications., in: Proceedings of the 28th International Symposium on Ballistics, 2014, p. 10.

[27] L. H. Nguyen, T. R. Lässig, S. Ryan, W. Riedel, A. P. Mouritz, A. C. Orifici, Numerical modelling of ultra-high molecular weight polyethylene composite under impact loading, Procedia Engineering 103 (2015) 436–443.

[28] J. A. Rogers, A. Mote, P. T. Mead, K. Harrison, G. D. Lukasik, K. R. Kota, W. D. Kulatilaka, J. W. Wilkerson, T. E. Lacy, Hypervelocity impact response of monolithic UHMWPE and HDPE plates, International Journal of Impact Engineering 161 (2022) 104081. doi:https://doi.org/10.1016/j.ijimpeng.2021.104081.

[29] EPIC dynamic finite element code (Oct 2021).
URL https://www.swri.org/industry/ballistics-explosives/epic-dynamic-finite-element-code

[30] G. R. Johnson, Analysis of Elastic-Plastic Impact Involving Severe Distortions, Journal of Applied Mechanics 43 (3) (1976) 439–444. doi:10.1115/1.3423887.

[31] G. R. Johnson, R. A. Stryk, T. J. Holmquist, O. A. Souka, Recent EPIC code developments for high velocity impact: 3D element arrangements and 2D fragment distributions, International Journal of Impact Engineering 10 (1) (1990) 281–294. doi:https://doi.org/10.1016/0734-743X(90)90066-5.

[32] J. Rogers, P. T. Mead, J. Wilkerson, T. E. Lacy, N. Williams, Simulating hypervelocity impacts to high-density polyethylene, in: AIAA SCITECH 2023 Forum, 2023, p. 2021.

[33] J. A. Rogers, N. Bass, P. T. Mead, A. Mote, G. D. Lukasik, M. Intardonato, K. Harrison, J. D. Leaverton, K. R. Kota, J. W. Wilkerson, J. N. Reddy, W. D. Kulatilaka, T. E. Lacy, The Texas A&M university hypervelocity impact laboratory: A modern aeroballistic range facility, Review of Scientific Instruments 93 (8) (2022) 085106. doi:10.1063/5.0088994.
URL https://doi.org/10.1063/5.0088994

[34] King Plastic Corporation, North Port, FL, King Performance Commodities HDPE: material and physical datasheet (2014).
URL https://www.kingplastic.com/wp-content/uploads/2014/05/King-KPC-HDPE-Physical-Properties.pdf

[35] D. Brown, R. M. Hanson, W. Christian, Tracker Video Analysis and Modeling Tool for Physics Education (V5.1.5) (2021).
URL https://physlets.org/tracker/

[36] G. R. Johnson, R. A. Stryk, S. R. Beissel, T. J. Holmquist, An algorithm to automatically convert distorted finite elements into meshless particles during dynamic deformation, International Journal of Impact Engineering 27 (10) (2002) 997–1013.

[37] G. R. Johnson, A constitutive model and data for materials subjected to large strains, high strain rates, and high temperatures, Proc. 7th Inf. Sympo. Ballistics (1983) 541–547.

[38] G. R. Johnson, W. H. Cook, Fracture characteristics of three metals subjected to various strains, strain rates, temperatures and pressures, Engineering fracture mechanics 21 (1) (1985) 31–48.

[39] E. Grüneisen, Theorie des festen zustandes einatomiger elemente, Annalen der Physik 344 (12) (1912) 257–306.

[40] B. J. Kohn, Compilation of hugoniot equations of state, Tech. rep., AIR FORCE WEAPONS LAB KIRTLAND AFB NM (1969).

[41] S. Marsh, Los alamos series on dynamic material properties (1980).

[42] RGP Balls, 20092 Cinisello Balsamo, Milan, Italy, RGP Balls: Aluminum Alloy Balls Series 1XXX material datasheet (2022).
URL https://www.rgpballs.com/

[43] E. Brown, R. Willms, G. Gray, P. Rae, C. Cady, K. Vecchio, J. Flowers, M. Martinez, Influence of molecular conformation on the constitutive response of polyethylene: a comparison of HDPE, UHMWPE, and PEX, Experimental mechanics 47 (3) (2007) 381–393.

[44] J. L. Jordan, D. T. Casem, J. Robinette, Hugoniot and dynamic strength in polyurea, Journal of Applied Physics 131 (16) (2022) 165903.

[45] J. Ahrens, B. Geveci, C. Law, ParaView: An End-User Tool for Large Data Visualization, Visualization Handbook, Elsevier, 2005.

[46] C. E. Anderson Jr, Analytical models for penetration mechanics: a review, International Journal of Impact Engineering 108 (2017) 3–26.

[47] A. J. Piekutowski, K. L. Poormon, Effects of scale on the performance of whipple shields for impact velocities ranging from 7 to 10 km/s, in: Procedia Engineering, Vol. 58, Elsevier Ltd, 2013, pp. 642–652. doi:10.1016/j.proeng.2013.05.074.

[48] E. L. Christiansen, J. H. Kerr, Ballistic limit equations for spacecraft shielding, International Journal of Impact Engineering 26 (1-10) (2001) 93–104.

[49] C. R. Siviour, J. L. Jordan, High strain rate mechanics of polymers: a review, Journal of Dynamic Behavior of Materials 2 (1) (2016) 15–32.

Appendix A. Supporting Plots

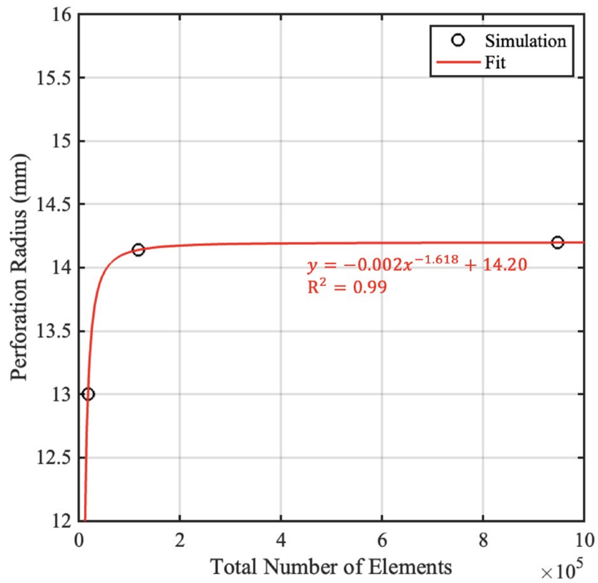

Figure A.1: Results of the mesh refinement analysis conducted in this study. The simulation convergence with respect to the number of elements is illustrated by fitting a two-term power law to the calculations.

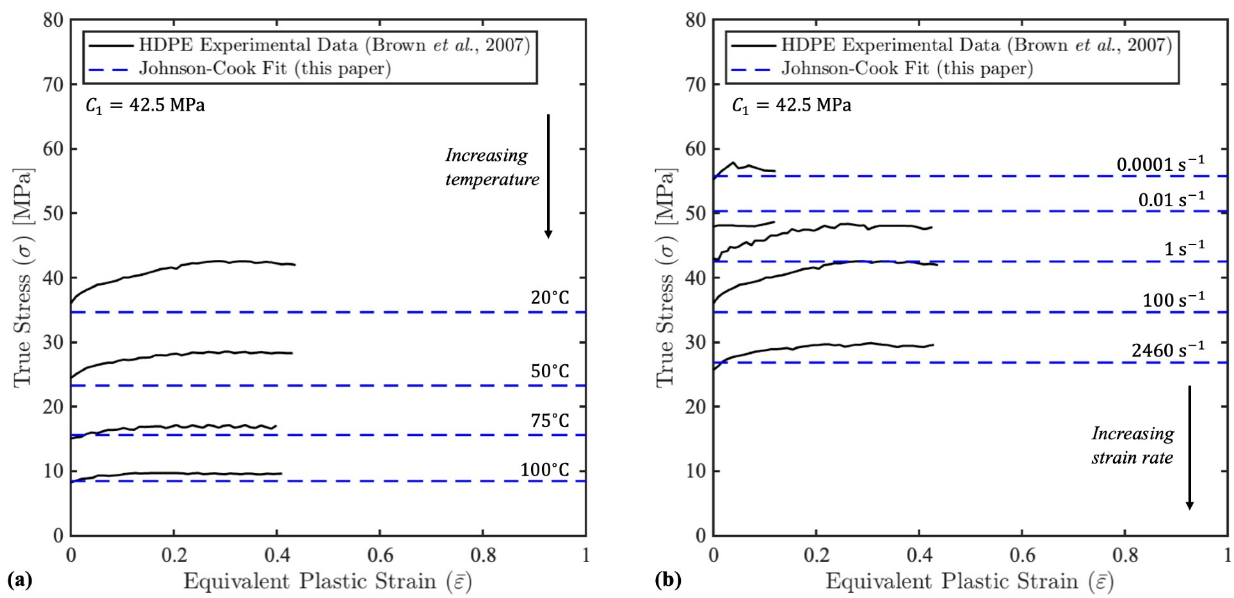

Figure A.2: Comparison of the Johnson-Cook (JC) constitutive model fit for HDPE with experimental data. The plots illustrate the model's capability to capture HDPE's (a) thermal softening and (b) strain rate hardening. The HDPE studied by Brown *et al.* [43] had a yield stress parameter (C_1) of 42.5 MPa, whereas the HDPE in this study had a C_1 value of 31.3 MPa (*cf.* Table 2). Consequently, the JC model fitting was initially performed with C_1 set to 42.5 MPa to determine the parameters m, N, C_2, and C_3. The C_1 value was then adjusted to 31.3 MPa to align the model more accurately with the experimental response of the HDPE used in this study, effectively shifting the plots downward.

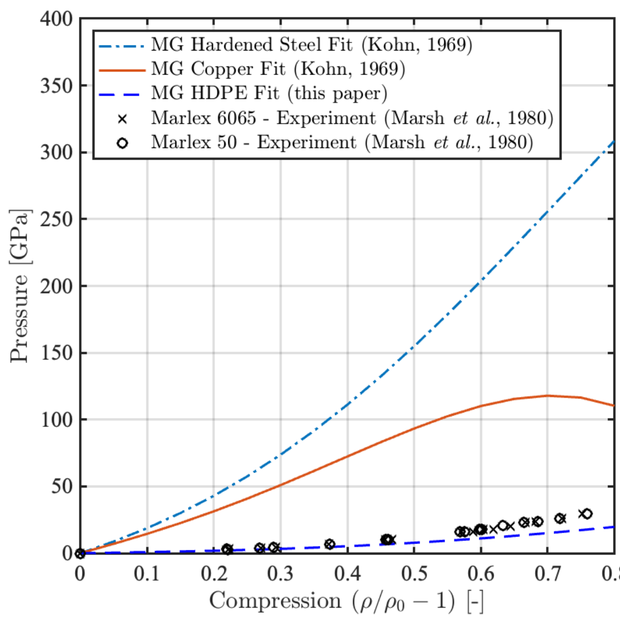

Figure A.3: Comparison of Hugoniot data for Marlex from Marsh *et al.* [41] with predictions from the Mie–Grüneisen (MG) equation of state (EOS) used in this study. Despite differences in properties between the simulated HDPE and Marlex 50 and 6050, the MG EOS fit from this study is comparable to the Hugoniot data for Marlex obtained from experiments. The plot also includes MG EOS fits for steel and copper from Ref. [40] to highlight the significant differences in pressure-volume responses between key metals and the thermoplastics.